Optically adjustable light filaments generated by a compact laser convertor

V. Kollárová[1], T. Medřík[1], R. Čelechovský[1], V. Chlup[1], Z. Bouchal[1*], A. Pochylý[2], M. Kalman[2], and T. Kubina[2]

[1]*Department of Optics, Palacký University, 17. listopadu 50, 772 07 Olomouc, Czech Republic*

[2]*Meopta-optika, s.r.o., Kabelíkova 1, 750 02 Přerov, Czech Republic*

[*]*Corresponding author:bouchal@optics.upol.cz*

Abstract: In the paper, light filaments realized as extremely narrow pseudo-nondiffracting beams with the spot size of several micrometers are examined. Attention is focused on their physical properties, attainable geometrical and energetic parameters and on the optical method enabling continuous relocation of the beam spot across the transverse plane. Testing of the laser convertor designed to realize adjustable minisized pseudo-nondiffracting beams is described and discussed. Experimental results approving useability of the set-up for optical transport of microparticles along a desired trajectory are also presented.

References and links

1. C. J. R. Sheppard and T. Wilson, "Gaussian-beam theory of lenses with annular aperture," Microwaves Opt. Acoustics 2, 105 (1978).
2. J. Durnin, J. J. Micely, and J. H. Eberly, "Diffraction-free beams," Phys. Rev. Lett. 58, 1499-1501 (1987).
3. W. C. Soares, D. P. Caetano, and J. M. Hickmann, "Hermite-Bessel beams and the geometrical representation of nondiffracting beams with orbital angular momentum," Opt. Exp. 14, 4577-4582 (2006).
4. J. C. Gutiérrez-Vega, M. D. Iturbe-Castillo, and S. Chávez-Cerda, "Alternative formulation for invariant optical fields: Mathieu beams," Opt. Lett. 25, 1493-1495 (2000).
5. M. A. Bandres, J. C. Gutiérrez-Vega, and S. Chávez-Cerda, "Parabolic nondiffracting optical wavefields," Opt. Lett. 29, 44-46 (2004).
6. Z. Bouchal, "Controlled spatial shaping of nondiffracting patterns and arrays," Opt. Lett. 27, 1376-1378 (2002).
7. Z. Bouchal, "Nondiffracting optical beams: physical properties, experiments, and applications," Czech. J. Phys. 53, 537 (2003).
8. M. R. Lapointe, "Review of non-diffracting Bessel beam experiments", Opt. & Laser Technol. 24, 315-321 (1992).
9. Z. Bouchal, "Physical principle of experiments with pseudo-nondiffracting fields," Czech. J. Phys. 55, 1223-1236 (2005).
10. V. Bagini, F. Frezza, M. Santarsierro, G. Schettini, and G. S. Spagnolo, "Generalized Bessel-Gauss beams", J. Mod. Opt. 43, 1155 (1996).
11. J. C. Gutiérrez-Vega and M. A. Bandres, "Helmholtz-Gauss waves," J. Opt. Soc. Am. A 22, 289 (2005).
12. Z. Bouchal, R. Čelechovský, and G. Swartzlander, Jr., "Spatially localized vortex structures," Monograph Localized waves, edited by H. E. Hernndez-Figueroa, M. Zamboni - Rached and E. Recami, J. Wiley & Sons., Inc. (in print).
13. V. Garcés-Chávez, D. McGloin, H. Melville, W. Sibbett, and K. Dholakia, "Simultaneous micromanipulation in multiple planes using a self-reconstructing light beam," Nature 419, 145-147 (2002).
14. T. Čižmár, V. Garcés-Chávez, K. Dholakia, and P. Zemánek, "Optical coveyor belt for delivery of submicron objects," Appl. Phys. Lett. 86, 174101-1-3 (2005).
15. J. Arlt, V. Garcés-Chávez, W. Sibbett, and K. Dholakia, "Optical micromanipulation using a Bessel light beam," Opt. Commun. 197, 239-245 (2001).

16. J. E. Curtis, B. A. Koss, and D. G. Grier,"Dynamic holographic optical tweezers," Opt. Commun. 207 169-175 (2002).
17. T. Čižmár, V. Kollárová, X. Tsampoula, F. Gunn-Moore, W. Sibbett, Z. Bouchal, and K. Dholakia, "Generation of multiple Bessel beams for a biophotonics workstation," Opt. Exp. (submitted).

1. Introduction

During two last decades, an increasing attention has been focused on physical properties, experimental realization and applications of nondiffracting (ND) beams. In an exact mathematical treatment, the monochromatic ND beams can be established as solutions of the Helmholtz equation. The complex amplitude of the ND beam then can be described by the well-known mathematical functions obtained applying the separation of variables in the convenient coordinate systems [1, 2, 3, 4, 5]. An illustrative explanation of the creation of the ideal ND beam provides Fourier optics. In this case, the ND beam can be comprehended as an interference field created by plane waves whose wave vectors $\mathbf{k} \equiv (k_x, k_y, k_z)$ have the same projection to the direction of the beam axis, $k_z = const$. The plane-wave components of the beam then change the phase in exactly the same way so that their interference pattern representing the beam intensity profile does not change under free-space propagation. The condition of the ND propagation puts a restriction on propagation directions of the plane-wave components of the spatial spectrum of the ND beam but admits an arbitrary amplitude and phase offset of each component. A targeted amplitude and phase modulation of the spatial spectrum enables the beam transformation important for its practical use. For example, the intensity profile of the ND beam can be shaped to a predetermined form or an array of the ND beams can be created [6, 7]. In an ideal case, the intensity profile of the ND beam is independent of the propagation coordinate and remains unchanged from $-\infty$ to $+\infty$. Its size can be adjusted in a wide interval by changing the angle which the wave vectors of the plane-wave components make with the beam axis. In an extreme case, the ND beam has a form of an infinite light filament with the diameter approximately equal to the wavelength of the used radiation. A conception of the ND propagation of light has only a theoretical meaning and cannot be directly connected with real experiments. The reason is an infinite energy covered by the cross-section of the ideal ND beam. In experiments realized by means of the annular amplitude mask, the axicon, the diffractive optical element or the computer generated hologram sent to the spatial light modulator [8, 9], the so-called pseudo-nondiffracting (P-N) beam can be generated. In its mathematical model, the transverse amplitude profile of the beam is bounded by a square integrable envelope so that the energy carried by the P-N beam is finite [10]. Under convenient experimental conditions the realizable P-N beams represent a good approximation of the theoretical ND beams.

In the paper, the geometry and energetics of the minisized P-N beams of the Bessel-Gauss (B-G) type are examined. The particular attention is focused on a method enabling continuous relocation of the beam spot across the allocated area of the transverse plane. The principle of the method is based on the phase modulation of the spatial spectrum. In the paper, the mathematical explanation of the beam spot relocation to the off-axis position is presented and its optical realization is proposed. The optical set-up enabling conversion of the fiber mode to the B-G with the adjustable spot is designed and realized as a compact laser convertor. Experimental results obtained by testing of the convertor are also presented. A possibility to connect the laser convertor to the optical tweezer and to use it for optical manipulations is verified and discussed.

2. Conception of nondiffracting propagation of light

2.1. Theoretical nondiffracting beam

In a scalar approximation, the ideal monochromatic ND beam can be comprehended as a mode-like field propagating along the well defined direction (z-axis). Its complex amplitude U_N can be written as a product of the transverse amplitude profile u_N and the phase oscillating term appointed by the propagation constant k_z,

$$U_N(\mathbf{r}) = u_N(x,y;k_t)\exp(-ik_z z). \tag{1}$$

Intensity profile of the ND beam $I = |u_N|^2$ remains unchanged during propagation and its dimensional scale depends on the parameter k_t, that can be expressed by means of the wave number k as $k_t^2 = k^2 - k_z^2$. The spatial spectrum of the ND beam is reduced to a single radial spatial frequency so that it can be expressed by the Dirac delta-function $\delta(k_x^2 + k_y^2 - k_t^2)$ in the k-space. If Eq. (1) is substituted into the Helmholtz equation, the admissible profiles of the nondiffracting beams u_N can be found applying the separation of variables in the Cartesian, circular cylindrical, elliptical cylindrical or parabolic cylindrical coordinates [11]. By this way, the nondiffracting fields known as the Bessel, Hermite-Bessel, Mathieu and parabolic beams can be obtained.

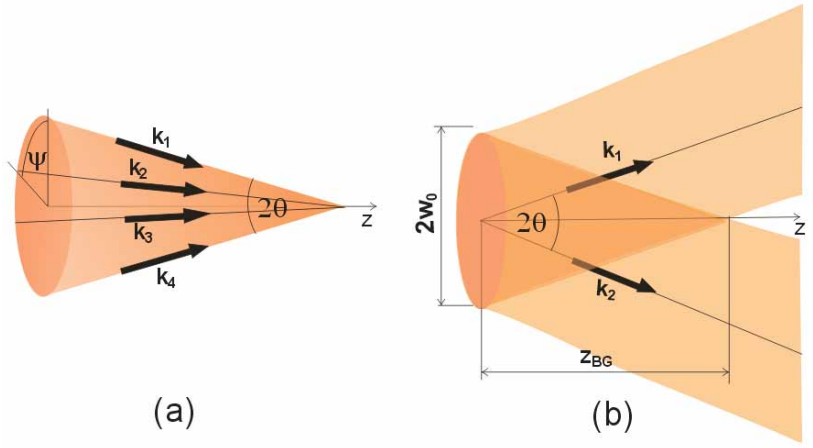

Fig. 1. Optical beams illustrated as interference field: (a) theoretical ND beam, (b) realizable P-N beam.

The ND propagation of light can be explained and clearly demonstrated if the ND beam is considered to be an interference field of plane waves with specially chosen propagation directions. The complex amplitude of the separate plane waves is given as $U_{PW}(\mathbf{r}) = a\exp(-i\mathbf{k}_t\cdot\mathbf{r}_t - ik_z z + i\Phi)$, where $\mathbf{k}_t \equiv (k_x,k_y)$, $\mathbf{r} \equiv (\mathbf{r}_t,z)$, $\mathbf{r}_t \equiv (x,y)$, a is a constant amplitude and Φ denotes a phase offset. The ND propagation is ensured only if the longitudinal component of the wave vector k_z is the same for all plane-wave components of the beam. This condition implies that also the magnitude of the transverse vector $\mathbf{k}_t$ is constant even if its direction changes for separate plane waves in dependence on the angle ψ (Fig. 1 a). If we assume that the ND field rises from a continuous superposition of plane waves, their wave vectors create a conical surface whose axis coincides with the propagation direction of the ND field. The vertex angle of the cone 2θ is simply related to the transverse and longitudinal components of the wave vector, $k_t = k\sin\theta$, $k_z = k\cos\theta$. Change of the angle θ causes dimensional scaling of the transverse intensity spot of the ND beam. If θ increases, the ND beam becomes narrower.

If the geometry of the interfering waves is described in the circular cylindrical coordinates, $x = \rho\cos\vartheta$, $y = \rho\sin\vartheta$, $k_x = k_t\cos\psi$ and $k_y = k_t\sin\psi$, the ND field U_N is obtained by integration of the plane waves U_{PW} along the azimuthal angle,

$$U_N(\mathbf{r}) = \exp(-ik_z z)\int_0^{2\pi} A(\psi)\exp[-ik_t\rho\cos(\vartheta-\psi)]d\psi, \tag{2}$$

where $A(\psi) = a(\psi)\exp[i\,\Phi(\psi)]$. The dependence of a and Φ on ψ means that the the amplitude and the phase offset can differ for separate plane waves. In general, $A(\psi)$ is an arbitrary periodical complex function. Its choice can be utilized for shaping of the beam intensity but it does not disturb the ND propagation of the beam. The azimuthal modulation of interfering plane waves is exploitable for generation of very complex ND fields including single or composed vortex fields, arrays of ND beams or ND fields with a predetermined shape [6, 7]. An admissible variability of $A(\psi)$ can also be used for a controllable transverse relocation of the beam spot [9]. If the amplitude $A(\psi)$ is replaced by

$$A(\psi) \rightarrow A(\psi)\exp[ik_t(\Delta x\cos\psi + \Delta y\sin\psi)], \tag{3}$$

the obtained ND beam preserves its shape and propagation direction but its center is transversely shifted to the position given by coordinates $[\Delta x, \Delta y]$. The complex amplitude of the beam is then given by $U_N(x-\Delta x, y-\Delta y, z)$. The required phase change of the angular spectrum (3) can be simply realized optically. It was utilized in design of the laser convertor enabling generation of adjustable light filaments. In a special case, the amplitude a and the phase offset Φ are constant for all plane waves used in the continuous superposition. Their interference then results in the well-known zero-order Bessel beam [1, 2].

2.2. Realizable pseudo-nondiffracting beams

The ND beam whose transverse intensity profile remains exactly invariable during propagation is an unattainable idealization. To simulate the experimentally realizable beam, the theoretical ND beam must be transversely bounded. In this case, the intensity asymptotically vanishes faster than $1/\rho^2$, where ρ is the transversal distance from the center of the beam. As a result, the P-N beam carrying finite energy is obtained. A simple and practically applicable model of the P-N beam is obtained if the bounding envelope has a Gaussian form. In this case, description of the P-N beam follows from the Helmholtz equation solved in the paraxial approximation. In the circular cylindrical coordinates, the well-known B-G beam is obtained as a realizable approximation of the theoretical Bessel beam. The P-N beam with a general intensity profile can be introduced applying the integral representation. In this case, the P-N beam can be comprehended as an interference field of inclined monochromatic Gaussian beams G whose axes create a conical surface with the vertex angle 2θ [10] (Fig. 1 b). The axes of the separate Gaussian beams are specified by the angles θ and ψ and their amplitudes are given by $A(\psi)$. The complex amplitude of the P-N field then can be expressed as

$$U_{PN}(\rho,\vartheta,z) = \int_0^{2\pi} A(\psi)G(\rho,\vartheta,z,\psi)d\psi. \tag{4}$$

The Gaussian beams under the integral can be specified by the complex parameter q defined by the confocal parameter q_0 as $q = z + iq_0$. The complex amplitude U_{PN} then becomes [12]

$$U_{PN}(\rho,\vartheta,z) = \exp\left(-i\frac{k_t^2 z^2}{2kq}\right)U_G(\rho,z)U(Q\rho,\vartheta,z), \tag{5}$$

where U_G denotes the Gaussian envelope and U is given as

$$U(Q\rho,\vartheta,z)=\exp(-ik_{zp}z)\int_0^{2\pi}A(\psi)\exp[-ik_tQ\rho\cos(\vartheta-\psi)]d\psi. \tag{6}$$

As is obvious, U has a form of the ND beam (2) where the propagation constant k_{zp} is replaced by its paraxial approximation

$$k_{zp}=k\left(1-\frac{{k_t}^2}{2k^2}\right), \tag{7}$$

and the variable ρ is replaced by a scaled variable $Q\rho$. The field intensity is not propagation invariant because except of the oscillating term also the complex scaling factor Q depends on the propagation coordinate,

$$Q=1+\frac{z}{q}. \tag{8}$$

The Gaussian envelope can be expressed by means of the standard parameters w_0, R and Ω representing the beam waist radius, the wavefront radius and the Gouy phase shift, respectively,

$$U_G(\rho,z)=\frac{w_0}{w}\exp\left(-\frac{\rho^2}{w^2}-i\frac{k\rho^2}{2R}+i\Omega\right), \tag{9}$$

where

$$w = w_0\left(1+\frac{z^2}{q_0^2cos^2\theta}\right)^{1/2}, \tag{10}$$

$$R = \frac{z}{\cos\theta}+\frac{q_0^2\cos\theta}{z}, \tag{11}$$

$$\Omega = \arctan\left(\frac{z}{q_0\cos\theta}\right). \tag{12}$$

A clear explanation of the differences between the ND and P-N beams can be demonstrated in terms of the Fourier optics. As was shown, the ND beam is in fact an interference field produced by the plane-wave components of the spatial spectrum given by the single radial spatial frequency $\nu=\sin\theta/\lambda$. In real experimental conditions, the interference field is not created by the plane waves with an infinite extent but by bounded waves. Therefore, the spatial spectrum is not limited to the single radial spatial frequency but it spreads to an annular area. The model of the P-N beams represents the experimentally realized beams very well. The beams can be simply created by means of an axicon or an annular mask placed at the front focal plane of a lens. Advanced experiments enabling generation of the P-N beams are based on application of the holographical element or the spatial light modulator.

3. Properties of minisized pseudo-nondiffracting beams

The ND and P-N beams represent a very wide group of optical fields with different intensity profiles and various physical properties. In the paper, the beams of the Bessel and B-G type are examined. Such beams were successfully applied to various laser tweezer experiments demonstrating simultaneous micromanipulation in multiple planes [13] or trapping and subsequent precise delivery of several submicron particles over a distance of hundreds of micrometers [14]. The B-G beams were also verified to be well suited to rotationally align rod-like particles along

the beam direction and to build and manipulate stacks of particles [15]. In the paper, attention is focused on geometrical parameters and energetics of the B-G beam and on optical means enabling relocation of the beam intensity spot across the transverse plane. An expediency of the B-G beams for their utilization in optical manipulation is discussed and demonstrated on comparison of parameters of the B-G and Gaussian beams.

3.1. Geometrical parameters

The complex amplitude of the ND and P-N beams can be expressed by the integrals (2) and (6) in which an arbitrary periodic function $A(\psi)$ appears. If it represents the phase modulation given as $A(\psi) = \exp(im\psi)$, $m = 0, \pm 1, \pm 2, \cdots$, the integral (2) results in

$$U_N(\rho, \vartheta, z) = (-1)^m i^m 2\pi J_m(k_t \rho) \exp(im\vartheta - ik_z z), \tag{13}$$

where J_m denotes the m-th order Bessel function of the first kind. If the same azimuthal phase modulation $A(\psi)$ is applied to the integral providing the P-N beam, its complex amplitude U_{PN} can be expressed by (5) with U given by

$$U(Q\rho, \vartheta, z) = (-1)^m i^m 2\pi J_m(k_t Q\rho) \exp(im\vartheta - ik_{zp} z). \tag{14}$$

In this case, the B-G beam is obtained. Its transverse amplitude profile is described by the Bessel function J_m bounded by the Gaussian function U_G. For $m \neq 0$, the Bessel and B-G beams are dark at the axis. They have a helical wavefront and belong to the group of optical vortices. In the paper, the bright zero-order Bessel and B-G beams ($m = 0$) are examined. In the case of the zero-order Bessel beam, the normalized intensity can be written as

$$I_N(\rho) \equiv \frac{|U_N(\rho)|^2}{|U_N(0)|^2} = J_0^2(k_t \rho). \tag{15}$$

As a member of the group of the theoretical ND beams, the zero-order Bessel beam reaches from $-\infty$ to $+\infty$. The beam is unbounded and carries an infinite energy. In the case of the B-G beam with the complex amplitude U_{BG}, the normalized intensity is defined by

$$I_{BG}(\rho, z) \equiv \frac{|U_{BG}(\rho, z)|^2}{|U_{BG}(0,0)|^2}. \tag{16}$$

By means of (5), it can be rewritten to the form

$$I_{BG}(\rho, z) = \frac{w_0^2}{w^2} \exp\left[-\frac{2\rho^2}{w^2} - \frac{k_t^2 z^2 q_0}{k(z^2 + q_0^2)}\right] J_0(k_t Q\rho) J_0(k_t Q^* \rho). \tag{17}$$

At the plane $z = 0$, the beam is expressed as the ideal Bessel beam bounded by the Gaussian envelope,

$$I_{BG}(\rho, 0) = J_0^2(k_t \rho) \exp\left(-\frac{2\rho^2}{w_0^2}\right). \tag{18}$$

The Bessel function J_0 defines intensity profile resembling the well-known Airy diffraction pattern. Its central disk has the radius given by $\rho_0 = 2.4/k_t$. If ρ_0 is small in comparison with the waist radius of the Gaussian envelope w_0, the B-G beam well approximates the ideal Bessel beam in a finite propagation region. Its length z_{BG} depends on w_0 and in experiments it can be changed for beams with the same ρ_0. The length of the region where the B-G beam exists can be examined by means of the axial intensity. Its normalized form can be written as

$$I_{BG}(0, z) = \frac{w_0^2}{w^2} \exp\left[-\frac{k_t^2 z^2 q_0}{k(z^2 + q_0^2)}\right]. \tag{19}$$

For propagation distances of interest which are considerably shorter than the Rayleigh distance of the Gaussian envelope, $z << q_0$, the axial intensity can be simplified to the form

$$I_{BG}(0,z) = \exp\left(-\frac{2z^2 \sin^2\theta}{w_0^2}\right). \tag{20}$$

The maximal propagation distance z_{BG} can be defined by means of an admissible decrease of the normalized axial intensity, $I_{BG}(0,z_{BG}) = 1/e^2$. The length of the usable propagation region of the B-G beam then can be written as

$$z_{BG} = \frac{w_0}{\sin\theta} \approx \frac{w_0}{\theta}. \tag{21}$$

As is obvious, the length of the B-G beam with the fixed size of the intensity spot ρ_0 is enlarged if the waist radius w_0 of the Gaussian envelope expands. This is unique property of the P-N beams unattainable with common laser beams. It can be successfully utilized for convey of

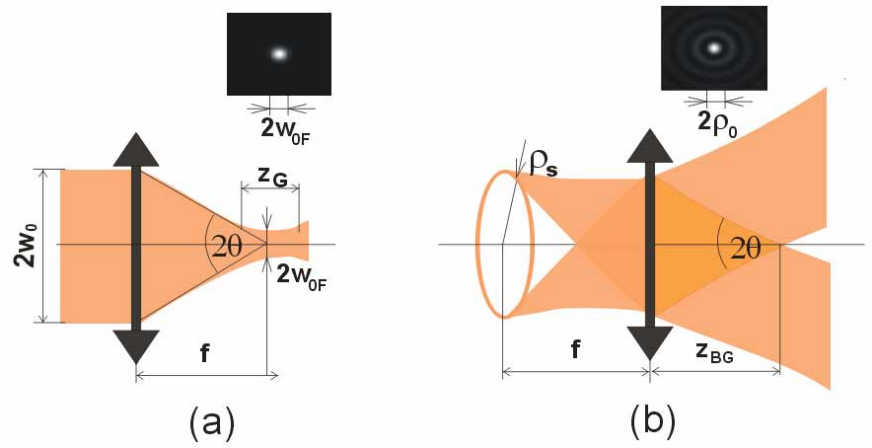

Fig. 2. Comparison of (a) the focused Gaussian beam and (b) the P-N beam of the B-G type.

micro-particles in optical manipulation where the narrow optical beams with a long propagation range are required. To demonstrate preferences of the P-N beams, the attainable parameters of the B-G and strongly focused Gaussian beams are compared under similar demands on optical elements used in the optical set-up (Fig. 2).

If the collimated Gaussian beam with the waist radius w_0 impinges on the lens with the focal length f (Fig. 2a), it is focused to the spot with the waist radius w_{0F} given by

$$w_{0F} = \frac{2f}{kw_0}. \tag{22}$$

The transformed beam can be treated as well focused inside a region whose length z_G follows from definition of the Rayleigh distance,

$$z_G = kw_{0F}^2. \tag{23}$$

The angular divergence of the focused Gaussian beam θ_G can be written as

$$\theta_G = \frac{2}{kw_{0F}}. \tag{24}$$

To examine propagation properties of the B-G beam, a simple experiment illustrated in Fig. 2b is considered. In this case, the annular light source is placed at the front focal plane of the lens with the Gaussian transparency defined by the waist radius w_0. The spherical waves emitted by the source are transformed to the Gaussian beams whose propagation axes create a conical surface with the vertex angle 2θ. Behind the lens, the B-G beam is created by interference of the Gaussian beams. Its transverse amplitude profile can be approximated by the Bessel function J_0 bounded by the Gaussian envelope. The angle θ is connected with the radius of the central spot ρ_0 of the generated beam,

$$\theta = \frac{2}{k\rho_0}. \tag{25}$$

As is obvious, similar claims are posed on the lens when the focused Gaussian beam and the B-G beam are comparable in size,$w_{0F} = \rho_0$. In both cases the lens with the numerical aperture $NA \approx \theta = \theta_G$ must be used. It seems to be reasonable to compare the length of the propagation range of both types of beams just for this case. On the accepted assumption that the waist radius of the focused Gaussian beam is equal to the radius of the central spot of the B-G beam, the length of the region where the B-G beam maintains its intensity profile can be approximated by

$$z_{BG} = \frac{kw_0 w_{0F}}{2}. \tag{26}$$

The ratio of the propagation lengths of the B-G beam and the focused Gaussian beam of a comparable transverse size can be written as

$$K \equiv \frac{z_{BG}}{z_G} = \frac{w_0}{2w_{0F}}. \tag{27}$$

Important geometrical parameters of the examined beams can be approximately expressed by means of the focal length f and the numerical aperture of the lens $NA = w_0/f$,

$$w_{0F} = \rho_0 = \frac{2}{kNA}, \tag{28}$$

$$z_G = \frac{4}{kNA^2}, \tag{29}$$

$$z_{BG} = f, \tag{30}$$

$$K = \frac{kfNA^2}{4}. \tag{31}$$

As is obvious, an elongation of the propagation region of the B-G beam in comparison with the Gaussian beam of comparable size is limited by the geometrical parameters f and NA of the available lens. As an example, the light beams with wavelength $\lambda = 0.5$ μm transformed by the lens with $f = 10$ mm and $NA = 0.5$ can be compared. In this case, the waist radius of the Gaussian beam and the radius of the central spot of the B-G beam are equal, $w_{0F} = \rho_0 \approx 0.3\,\mu$m. While the Gaussian beam remains focused in the range of length only $z_G \approx 1.3$ μm, the B-G beam propagates with unchanged central spot through the distance $z_{BG} \approx 10$ mm. In this case, the propagation distance is approximately 7800 times longer for the B-G beam than for the Gaussian beam.

3.2. Efficiency of the power capture inside the beam propagation region

For the convey of microparticles in experiments with optical tweezers, the narrow optical beams with a long propagation distance are desirable. To compare various types of beams, their spatial

localization of the electromagnetic energy must be quantified. As a convenient measure, the fraction of the power captured by the detector of a given size and position can be accepted. To evaluate changes of the efficiency of the power detection inside the propagation region of the beam, the power captured by the detector with the radius R_D is explored in dependence on its position along the beam propagation direction. In this connection, the power capture coefficient η is defined as

$$\eta(z) = \frac{P_Z(z)}{P_0}, \tag{32}$$

where P_Z is the optical power received by the detector at the position specified by the longitudinal coordinate z and P_0 denotes the maximal power captured by the detector at the plane of the best transverse localization of the beam. In the case of the Gaussian beam, the power P_0 is related to the waist plane of the focused beam and P_Z denotes the power captured at the distance z from the waist plane. The power capture coefficient η_G is in this case defined by

$$\eta_G(z) = \frac{1-\exp\left(-2R_D^2/w^2\right)}{1-\exp\left(-2R_D^2/w_{0F}^2\right)}, \tag{33}$$

where

$$w^2 = w_{0F}^2 + \frac{z^2\lambda^2}{\pi^2 w_{0F}^2}. \tag{34}$$

For the B-G beam, the power capture coefficient can be obtained in an acceptable approximation. It is based on the assumption that the size of the detector is small in comparison with the waist radius of the Gaussian envelope, $R_D << w_0$. In this case, the Gaussian background appearing in I_{BG} given by (18) is approximately constant at the area of the detector and P_0 is given by

$$P_0 = 2\pi I_0 \int_0^{R_D} J_0^2(k_t\rho)\rho d\rho, \tag{35}$$

where I_0 is a constant intensity used for scaling of the total optical power carried by the beam. After integration we obtain

$$P_0 = \pi R_D^2 I_k \left[J_0^2(k_t R_D) + J_1^2(k_t R_D)\right]. \tag{36}$$

In the propagation range of the B-G beam, the size and shape of the central spot remain unchanged and only the axial intensity must be scaled due to redistribution of the energy in the side lobes. If the detector is placed inside the propagation region ($z < z_{BG}$), the captured power can be approximated by

$$P_Z = I_{BG}(0,z)P_0, \tag{37}$$

where $I_{BG}(0,z)$ is the axial intensity of the B-G beam given by (20). In the used approximation, the power capture efficiency of the B-G beam can be estimated as

$$\eta_{BG}(z) = I_{BG}(0,z). \tag{38}$$

To compare energetics of the Gaussian and B-G beams, it is useful to express a distance at which the power transfer efficiency falls to the given value η_G and η_{BG}, respectively. For the Gaussian beam it can be written as

$$z = \frac{z_G}{2}\sqrt{-1-\frac{2R_D^2}{w_{0F}^2 \ln V}}, \tag{39}$$

where

$$V = 1 - \eta_G \left[1 - \exp\left(-\frac{2R_D^2}{w_{0F}^2} \right) \right]. \tag{40}$$

For the B-G beam we obtain

$$z = z_{BG} \sqrt{-\frac{\ln \eta_{BG}}{2}}. \tag{41}$$

Changes of the efficiency of the power capture inside the propagation region of the Gaussian and B-G beams can be examined by (39) and (41). Similarly as in the example demonstrating the geometrical parameters of the beams we assume $\lambda = 0.5$ μm, $f = 10$ mm and $NA = 0.5$. In this case, the waist radius of the Gaussian beam is equal to the radius of the central spot of the B-G beam, $w_{0F} = \rho_0 = 0.3$ μm. In the analysis of the captured power, the detector with the radius comparable to the beam spot, $R_D = 0.3$ μm, is placed at the plane where the maximal power is detected. This choice was motivated by the fact that the B-G beams can manipulate particles whose size is comparable to the beam core. If the object is moved along the axis of the beam, some energy escapes due to diffraction effects and the captured power goes down. In the case of the focused Gaussian beam, the power falls to 80% on a very short distance of 1 μm. For the B-G beam, the power captured by the detector remains over 80% on a very long distance of more than 3 mm.

3.3. Optical transverse relocation of the beam spot

As follows from (2), the ND beam is created by interference of plane waves with the specified propagation directions and arbitrary amplitudes and phases. The amplitude and phase modulation $A(\psi)$ of the plane wave spectrum can be used for shaping of the beam intensity profile or for the targeted transverse relocation of the beam spot. If the amplitude of the separate plane waves is constant and their phase is modulated by

$$A(\psi) = \exp[ik_t(\Delta x \cos\psi + \Delta y \sin\psi)], \tag{42}$$

the complex amplitude of the created ND beam is proportional to the expression

$$U_N \propto \exp(-ik_z z)\ J_0\left[k_t \sqrt{(x-\Delta x)^2 + (y-\Delta y)^2} \right]. \tag{43}$$

In this case, the beam amplitude profile is described by the zero-order Bessel function. The beam spot remains unchanged in free propagation but its axis is transversely shifted to the position given by $[\Delta x, \Delta y]$. If the phase modulation (42) is used in (4), the B-G beam with the transversely relocated intensity spot is described. Unlike the theoretical Bessel beam, the spot of the B-G beam is nonsymmetricly bounded by the Gaussian envelope at the off-axis position. The intensity profiles of the theoretical Bessel beam and the realizable B-G beam are illustrated in Fig. 3. In experiments, the phase shift of the plane wave components (42) can be realized at the Fourier plane of the lens in the 4-f optical system illustrated in Fig. 4. The transformation can be simply explained for the case of the zero-order input Bessel beam whose axis coincides with the lens axis. The spatial spectrum of the beam created by the first Fourier lens has a shape of the bright circle with the radius ρ_S inversely proportional to the spot size of the input beam ρ_0. Alternatively, it can be expressed by the beam parameter k_t, $\rho_S \approx f k_t / k$, where f is the focal length of the lens. To perform required phase shift $A(\psi)$ of the separate plane wave components localized at the circle it is sufficient to place a wedge prism with the vertex angle α near the

Fig. 3. The intensity spot of the B-G beam at (a) the on-axis and (b) the off-axis positions.

focal plane of the lens. If the wedge prism is oriented along the *x*-axis as shown in Fig. 4, the phase modulation of the transmitted light can be approximately expressed by

$$t(\psi) = \exp[ik_t(n-1)\alpha f \cos\psi], \tag{44}$$

where n is the refractive index of the wedge prism and the insignificant constant phase shift was omitted. Interference of the light transmitted through the wedge prism creates the inclined divergent B-G beam [9]. By the second Fourier lens, it is transformed to the off-axis B-G beam. In the assumed theoretical case its complex amplitude is given by (43). From comparison of (42) with (44) it is clear that the wedge prism in the assumed orientation causes the transverse relocation of the beam spot to the position $(\Delta x, 0)$. The shift along the *x*-axis is given by

$$\Delta x = (n-1)\alpha f. \tag{45}$$

It is simple to show that the relocation of the beam spot to the arbitrary position $[\Delta x, \Delta y]$ can be ensured by means of the wedge prism with a variable vertex angle whose position can be changed by rotation around the lens axis. In experiments it can be realized by means of the diasporometer.

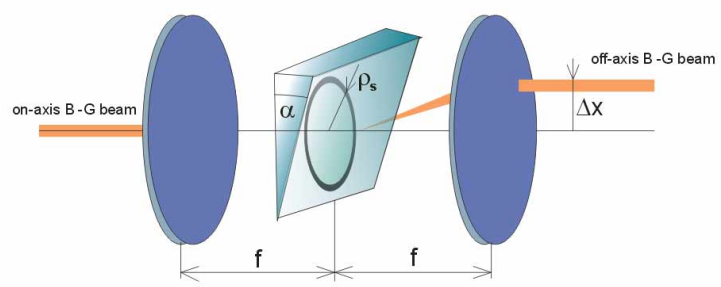

Fig. 4. Illustration of the phase modulation of the B-G beam spatial spectrum resulting in the transverse relocation of the beam spot.

4. Design of the laser beam converter

As was shown, the P-N beams possess unique propagation features interesting for applications. Their main advantage consists in (i) realization of an extremely narrow beam with a controllable length of the propagation range, (ii) achievement of the nearly constant efficiency of the

power capture inside the propagation region, (iii) possibility to relocate the beam spot by phase modulation of the spatial spectrum. In the paper, the design and realization of the laser convertor enabling generation of the adjustable P-N beam of the B-G type is described. The convertor is designed as a compact optical system illuminated by laser radiation guided by the optical fiber. As its output, the B-G beam of specified parameters is obtained. It has intensity spot of the required size whose shape remains unchanged in a long propagation region. The core axis of the beam is adjustable, it can be transversely relocated in a well defined area without changing direction. This action can be performed by a working movement of the optical diasporometer. Such beam is suitable for adjusting of optical elements because its directionality is well maintained for all transverse positions of the beam spot. By means of a simple auxiliary optical system, the B-G beam can be reduced to minisized beam with the core of several micrometers. In this configuration, the laser convertor works as the laser tweezer enabling conveying and transport of microparticles along desired trajectories. The movement of the optical traps is controlled by a simple action of the diasporometer.

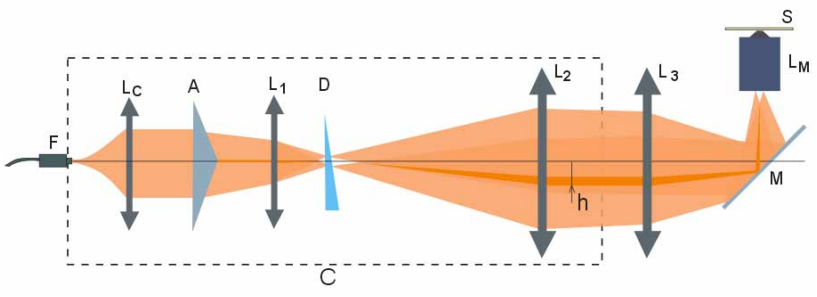

Fig. 5. Laser convertor C used in the set-up for conveying and transfer of microparticles along desired trajectory (F-fiber, L_C-collimating lens, A-axicon, D-diasporometer, L_1, L_2, L_3-lenses, M-mirror, L_M-microscope objective, S-sample).

Optical scheme of the designed laser convertor is illustrated in Fig. 5. The laser radiation leaving the optical fiber F is collimated by the lens L_C and directed to the axicon A. Behind the axicon, the B-G beam whose intensity profile can be approximated by the zero-order Bessel function bounded by the Gaussian envelope is created. The subsequent lenses L_1 and L_2 are placed so that they work as a telescope. The role of the telescope is dual - it scales the input beam and enables its relocation by the phase modulation introduced by the diasporometer placed at the back focal plane of the lens L_1. It is designed in such a way that can operate as a wedge prism with variable vertex angle rotating around the beam axis.

Though the B-G beam entering the telescope can be realized by several ways, the method using the axicon was chosen owing to its very good energetic efficiency. The radius ρ_1 of the spot size of the created beam depends on the axicon vertex angle τ and can be estimated by

$$\rho_1 \approx \frac{0.4\lambda}{(n-1)\left(\frac{\pi}{2}-\frac{\tau}{2}\right)} \tag{46}$$

where λ and n denote the wavelength of the used radiation and the refractive index of the axicon, respectively. The telescope composed of the lenses L_1 and L_2 scales the input beam in a measure depending on the magnification of the telescope given by the focal length of the lenses f_1 and f_2, $\Gamma_1 = -f_1/f_2$. The core radius of the beam behind the telescope then can be written

as

$$\rho_2 = \frac{\rho_1}{|\Gamma_1|}\sqrt{1-\left(\frac{0.4\lambda}{r_1}\right)^2(1-\Gamma_1^2)}. \tag{47}$$

The length of the propagation region of the beam created by the axicon z_1 depends on the axicon vertex angle and on its diameter. The telescope changes not only the spot size of the input beam but also its range. It can be expressed by means of the magnification as

$$z_2 = z_1/\Gamma_1^2. \tag{48}$$

The diasporometer simulating action of the wedge prism with the variable angle α causes the off-axis shift of the beam spot whose magnitude is given by

$$h = (n-1)\alpha f_2. \tag{49}$$

The direction of the shift is given by the azimuthal orientation of the wedge prism. To reduce the size of the beam to microscale, an additional telescope must be used. If the beam is to be exploited in optical manipulation, the telescope is composed of the auxiliary lens L_3 with the focal length f_3 and the microscope objective L_M with the focal length f_M. Changes of the beam spot size and the beam propagation range caused by the additional telescope are also given by (47) and (48) but the magnification Γ_1 must be replaced by $\Gamma_2 = -f_3/f_M$. The off-axis shift of the beam core h is reduced by the additional telescope to the value h/Γ_2.

5. Realization of the beam convertor and experimental results

After a dimensional design, the laser convertor shown in Fig. 5 was optimized by the standard optical software and parameters of its components were specified. In the convertor testing, the radiation of the He-Ne laser (632 nm, 15 mW) was brought by the optical fiber with the numerical aperture NA = 0.13 and mode field diameter MFD = 3.3 μm. The collimation of the input light was performed by the lens L_C with the focal length $f_C = 25.4$ mm. The B-G beam was created by the axicon with the vertex angle $\tau = 178^\circ$ (Eksma 130-0278). For the transverse relocation of the beam spot the diasporometer with the range of deviation angles $\pm 0.5^\circ$ was used. The transformation of the B-G beam was realized by the telescope composed of the lenses with the focal lengths $f_1 = 35$ mm and $f_2 = 250$ mm. The photo of the compact laser adapter is shown in Fig. 6a. The beam appearing behind the laser convertor has the core radius 200 μm and the length of existence about 14 m. It is applicable to the centering or adjusting of optical elements. Alternatively, a collimating lens with the larger focal length can be used. In this case the propagation range of the beam can be enlarged up to 20 m. The tranverse relocation of the beam core can be performed at the area of 4.5×4.5 mm^2. In performed experiment, the theoretical efficiency of the power capture inside the propagation region of the generated beam was also examined. The B-G beam created by the laser convertor was ten times dimensionally reduced by a telescope so that the radius of its core was approximately $\rho_0 = 20$ μm. The power captured by the detection area with the radius $R_D = \rho_0 = 20$ μm was measured for various positions inside the beam propagation region. It was performed in such a way that the reduced beam was imaged to the CCD camera and the accepted power was determined by means of the image processing. The obtained data enabled evaluation of the dependence of the coefficient η_{BG} defined by (38) and (20) on the propagation coordinate z. In Fig. 7, a very good agreement of the theoretical and experimental results is illustrated.

The laser convertor was also tested in the set-up for the manipulation of microparticles. In this case, the laser Verdi V2 (532 nm, maximal power 2 W) was used. The B-G beam leaving the convertor was dimensionally reduced by the additional telescope composed of the lens

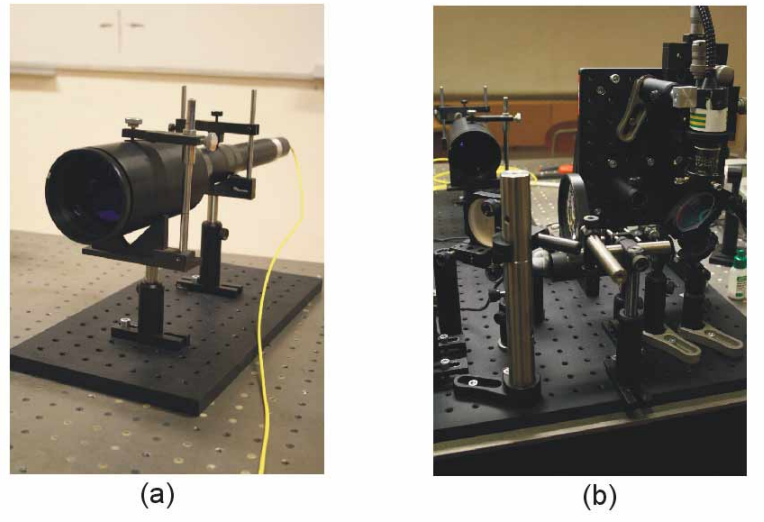

Fig. 6. Photos of (a) the compact laser adapter and (b) the set-up for conveying and transport of microparticles.

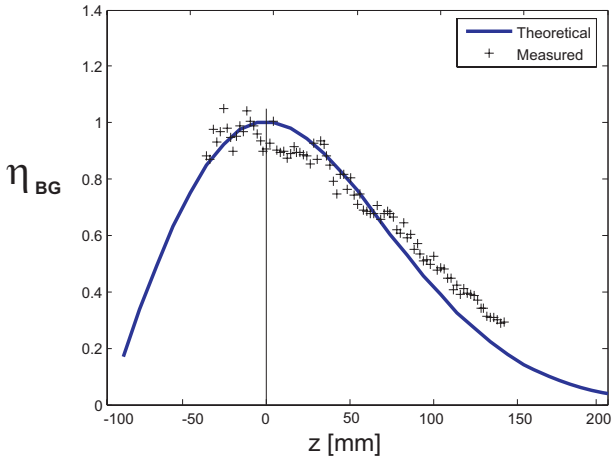

Fig. 7. Efficiency of the power capture inside the propagation region of the B-G beam.

$L3$ of the focal length $f_3 = 200$ mm and the microscope objective $f_M = 1.8$ mm (Olympus, UPLFLN 100×O2). The photo of the set-up is shown in Fig. 6b. The lowest power of the laser enabling optical manipulation was 60 mW, the power delivered to the created optical trap was approximately 50% of the light power leaving the fiber. The radius of the core of the beam in the optical tweezer is around $2\,\mu$m. By this beam we were able to catch, convey and shift the polystyrene particles (Duke Scientific) with diameter $5\,\mu$m at the area of $40 \times 40\,\mu\text{m}^2$. Results of the experiment are shown in Fig. 8. By means of the diasporometer, the particles were continuously transposed along the illustrated path. The snapshots illustrate the caught particles at the positions (a)-(f) of the defined trajectory. The small particles with the diameter around $1\,\mu$m could be conveyed, but not manipulated. After their catching and conveying, they

were stuck on the cover glass.

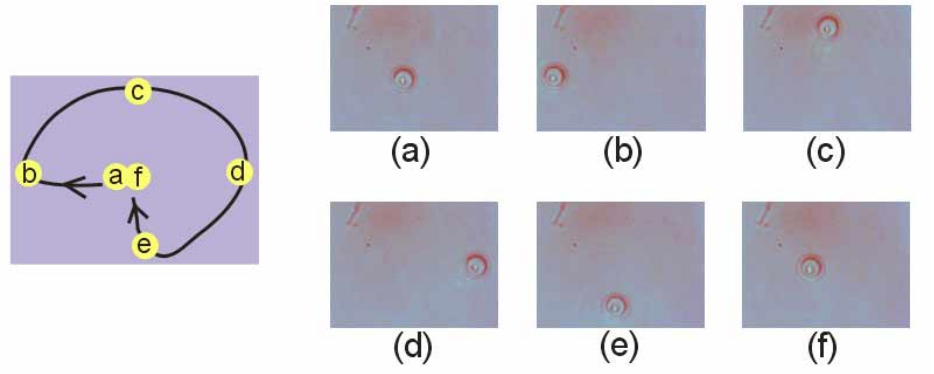

Fig. 8. Catching and movement of the polystyrene bead along a required trajectory by means of the set-up with the laser convertor.

6. Conclusion

In the paper, the geometrical and energetic parameters of the P-N beams of the B-G type were examined theoretically and experimentally. Their unique properties were utilized for realization of the experiment enabling conversion of the fiber mode to the long and narrow B-G beam whose axis can be transversely relocated at the defined area. The experimental set-up was optimized and produced as a compact laser convertor in the Meopta - optika company. The laser convertor was tested in real experimental conditions aimed for centering and adjusting of optical components. The particular attention was focused on a verification of the possibility to utilize the laser convertor as a device working as the laser tweezer enabling dynamical optical manipulation. In this case, the transverse relocation of the beam spot is controlled by a simple working movement of the diasporometer placed inside the laser convertor. By this way the particles with the diameter of several micrometers can be caught, conveyed and moved along the required trajectory. The realized set-up represents simpler and cheaper alternative of the holographical tweezers based on utilization of the spatial light modulator [16]. Some of the applications of the B-G beams demonstrated in the biophotonic workstation based on the use of the spatial light modulator [17] can be ensured with the set-up utilizing the laser convertor. The optical system of the laser convertor can be coupled with the spiral phase mask placed near the diasporometer. After this simple modification, the transversely movable optical vortices can be created. They can be applied to the promising experiments on the transfer of the orbital angular momentum to microparticles.

7. Acknowledgements

This work was supported by the Research projects Measurement and Information in optics MSM 6198959213, Center of Modern Optics LC06007 and project FT-TA2/059 of the Czech Ministry of Industry and Trade.